NASA Technical Memorandum 107707

ICASE Report No. 92–61

AD-A261 840

ICASE

PSEUDOSPECTRAL SIMULATION OF COMPRESSIBLE TURBULENCE USING LOGARITHMIC VARIABLES

John V. Shebalin

DTIC
S ELECTE
MAR 12 1993
E D

January 1993

Institute for Computer Applications in Science and Engineering
NASA Langley Research Center
Hampton, Virginia 23681–0001

Operated by the Universities Space Research Association

,iSTRIBU..JN STATEME
Approved for public release
Distribution Unlimited

NASA

National Aeronautics and
Space Administration

Langley Research Center
Hampton, Virginia 23681-0001

93-05249

98   3 11 079

Pseudospectral Simulation of Compressible Turbulence Using Logarithmic Variables

John V. Shebalin*

NASA Langley Research Center, Hampton, Virginia 23681

The direct numerical simulation of dissipative, highly compressible turbulent flow is performed using a pseudospectral Fourier technique. The governing equations are cast in a form where the important physical variables are the fluid velocity and the natural logarithms of the fluid density and temperature. Bulk viscosity is utilized to model polyatomic gases more accurately and to ensure numerical stability in the presence of strong shocks. Numerical examples include three-dimensional supersonic homogeneous turbulence and two-dimensional shock-turbulence interactions.

DTIC QUALITY INSPECTED 8

Accesion For		
NTIS CRA&I		☒
DTIC TAB		☐
Unannounced		☐
Justification		
By		
Distribution /		
Availability Codes		
Dist	Avail and / or Special	
A-1		

1 Introduction

The primary topic to be discussed in this paper is the direct numerical simulation of those highly compressible turbulent flows which can be described by the single-fluid Navier-Stokes equations within the constraint of periodic boundary conditions. While modern theoretical analyses of compressible turbulent flows began with the work of Moyal [1], their direct numerical simulation is much more recent. Following the seminal work of Passot and Pouquet [2], many other authors have also used Fourier methods, for example, Erlebacher *et al.*, [3], Blaisdell *et al.*, [4], Sarkar *et al.*, [5], Kida and Orszag [6], and Zang *et al.*, [7].

Here, Fourier methods are extended in two principal ways. First, we describe a technique which has proven useful previously [8]: the governing equations are cast in a form where the important physical variables are not the fluid density and temperature directly, but rather their natural logarithms; this ensures adherence to a physical constraint of positive-definiteness which may be computationally violated in non-logarithmic formulations, leading to numerical instability. Second, bulk viscosity is utilized, both to model polyatomic gases more accurately and concomitantly to ensure numerical stability in the presence of strong shocks.

The efficacy of using logarithmic variables and physical values of bulk viscosity will be shown through several numerical examples. In particular, logarithmic variables will allow for the simulation of supersonic homogeneous turbulent flow, while bulk viscosity will enable the resolution of shock structure. These numerical examples will be followed by a conclusion where extensions of the current work will be discussed.

2 Basic Equations

The basic equations of compressible fluid dynamics may be expressed as

$$\frac{\partial \rho}{\partial t} + \nabla \cdot \rho \mathbf{u} = 0 \tag{1}$$

$$\frac{\partial \rho \mathbf{u}}{\partial t} + \nabla \cdot \rho \mathbf{u}\mathbf{u} = -\nabla p + \nabla \cdot \left[\mu \nabla \mathbf{u} + \left(\frac{\mu}{3} + \mu_B \right) \mathbf{I} \nabla \cdot \mathbf{u} \right] \tag{2}$$

$$\frac{\partial p}{\partial t} + \nabla \cdot p \mathbf{u} = -(\gamma - 1)p \nabla \cdot \mathbf{u} + (\gamma - 1)\nabla \cdot (\kappa \nabla T)$$

$$+ (\gamma - 1) \left[\frac{\mu}{2} \tau_{ij} \tau_{ij} + \mu_B (\nabla \cdot \mathbf{u})^2 \right] \tag{3}$$

Here, $\tau_{ij} = \partial_i u_j + \partial_j u_i - 2/3\, \delta_{ij} \nabla \cdot \mathbf{u}$ and $\mathbf{I} = [\delta_{ij}]$ is the unit dyadic.

The equation of state will be that of an ideal gas, $p = R\rho T/m$, where $R/m = c_p - c_v$; R is the ideal gas constant, m is the molecular weight of the gas and c_p and c_v are the specific heats at constant pressure and volume, respectively. Here, we will consider *polytropic* gases, *i.e.*, gases such that the

specific heats and their ratio $\gamma = c_p/c_v$ are taken to be constants. In this case, the speed of sound c satisfies $c^2 = \gamma RT/m = \gamma p/\rho$.

We can non-dimensionalize the equations (1)–(3) in terms of reference values ρ_o, T_o, and u_o. Thus, using $c_o^2 = \gamma RT_o/m$ and $p_o = \rho_o c_o^2/\gamma$ we have (in the following, dimensionless quantities have a superscript attached, e.g., ρ^*):

$$\begin{aligned}
\rho &= \rho_o \rho^* \\
\mathbf{u} &= u_o \mathbf{u}^* \\
T &= T_o T^* \\
p &= p_o p^* = \rho_o c_o^2 \rho^* T^*/\gamma
\end{aligned} \tag{4}$$

Now we choose a length scale L_o so that $t = t_o t^*$ where $t_o = L_o/u_o$. Then dividing (1) by ρ_o/t_o, (2) by $\rho_o u_o/t_o$, and (using $R/m = c_v(\gamma - 1)$) dividing (3) by p_o/t_o gives:

$$\frac{\partial \rho^*}{\partial t^*} + \nabla_* \cdot \rho^* \mathbf{u}^* = 0 \tag{5}$$

$$\begin{aligned}
\frac{\partial \rho^* \mathbf{u}^*}{\partial t^*} + \nabla_* \cdot \rho^* \mathbf{u}^* \mathbf{u}^* = &-\frac{1}{M_o^2 \gamma} \nabla_* \rho^* T^* \\
&+ \nabla_* \cdot \left[\mu^* \nabla_* \mathbf{u}^* + \left(\frac{\mu^*}{3} + \mu_B^* \right) \mathbf{I}\, \nabla_* \cdot \mathbf{u}^* \right]
\end{aligned} \tag{6}$$

$$\begin{aligned}
\frac{\partial \rho^* T^*}{\partial t^*} + \nabla_* \cdot \rho^* T^* \mathbf{u}^* = &-(\gamma - 1)\rho^* T^* \nabla_* \cdot \mathbf{u}^* + \nabla_* \cdot (\kappa^* \nabla_* T^*) \\
&+ M_o^2 \gamma (\gamma - 1) \left[\frac{\mu^*}{2} \tau_{ij}^* \tau_{ij}^* + \mu_B^* (\nabla_* \cdot \mathbf{u}^*)^2 \right]
\end{aligned} \tag{7}$$

Here, $M_o = u_o/c_o$ is the reference Mach number and the dimensionless transport coefficients are:

$$\begin{aligned}
\mu^* &= \mu/(\rho_o u_o L_o) \\
\mu_B^* &= \mu_B/(\rho_o u_o L_o) \\
\kappa^* &= \kappa/(c_v \rho_o u_o L_o)
\end{aligned} \tag{8}$$

and the t_{ij}^* are the same as previously defined, except now in terms of the corresponding dimensionless quantities.

In (8), we recognize $\mu^* = 1/Re$, i.e., the dimensionless shear viscosity is the inverse of the Reynolds number Re. Although the transport coefficients which appear in the fluid equations are generally dependent on ρ or T or both, here we will operate under the assumption that these coefficients are all constant. Then the Prandtl number is $Pr = c_p \mu/\kappa = \gamma \mu^*/\kappa^*$ and the ratio of bulk to shear viscosity $\beta = \mu_B/\mu = \mu_B^*/\mu^*$ will also be constant.

Using the quantities developed above, we can write the dimensionless fluid equations in a more compact form. First, we will drop the '*' from the dimensionless quantities, remembering that we are now dealing with non-dimensional

2

equations. Second, we will choose the reference velocity as $u_o = c_o$ so that $M_o = 1$. Then, since γ, μ, μ_B, and κ are all constants, the equations become

$$\frac{\partial \rho}{\partial t} + \nabla \cdot \rho \mathbf{u} = 0 \tag{9}$$

$$\frac{\partial \rho \mathbf{u}}{\partial t} + \nabla \cdot \rho \mathbf{u}\mathbf{u} = -\frac{1}{\gamma}\nabla \rho T$$
$$+ \mu \nabla \cdot \left[\nabla \mathbf{u} + \left(\frac{1}{3} + \beta \right) \mathbf{I} \nabla \cdot \mathbf{u} \right] \tag{10}$$

$$\frac{\partial \rho T}{\partial t} + \nabla \cdot \rho T \mathbf{u} = -(\gamma - 1)\rho T \nabla \cdot \mathbf{u} + \kappa \nabla^2 T$$
$$+ \gamma(\gamma - 1)\mu \left[\frac{1}{2}\tau_{ij}\tau_{ij} + \beta(\nabla \cdot \mathbf{u})^2 \right] \tag{11}$$

(The dimensionless pressure is $p = \rho T/\gamma$.) These are the set of basic equations with which we will simulate the motion of a compressible fluid. In particular, by judiciously choosing appropriate values for μ, β, and κ, we will be able to simulate both turbulence and shocks, as well as their interaction.

3 Logarithmic Variables

Although the variables ρ and T may take values only between 0 and ∞, it is always possible in a discrete numerical simulation to inadvertently assign these variables non-positive values. When this occurs, an instability generally arises which stops the simulation. One sure way to avoid this is to express the basic equations in terms of *logarithmic variables*: $\lambda = \ln \rho$ and $\sigma = \ln T$. This is particularly appropriate when we wish to simulate fluid flows in which compressibility plays an important role, as in the case where shocks are present. Since this is the case at hand, we will use these logarithmic variables here.

Placing $\rho = e^\lambda$ and $T = e^\sigma$ into (9)–(11) yields the basic non-dimensional equations in a logarithmic formulation:

$$\frac{\partial \lambda}{\partial t} + \mathbf{u} \cdot \nabla \lambda = -\nabla \cdot \mathbf{u} \tag{12}$$

$$\frac{\partial \mathbf{u}}{\partial t} + \mathbf{u} \cdot \nabla \mathbf{u} = -\frac{1}{\gamma}e^\sigma \nabla(\lambda + \sigma)$$
$$+ \mu e^{-\lambda} \nabla \cdot \left[\nabla \mathbf{u} + \left(\frac{1}{3} + \beta \right) \mathbf{I} \nabla \cdot \mathbf{u} \right] \tag{13}$$

$$\frac{\partial \sigma}{\partial t} + \mathbf{u} \cdot \nabla \sigma = -(\gamma - 1)\nabla \cdot \mathbf{u} + \kappa e^{-\lambda}[\nabla^2 \sigma + (\nabla \sigma)^2]$$
$$+ \gamma(\gamma - 1)\mu e^{-(\lambda + \sigma)} \left[\frac{1}{2}\tau_{ij}\tau_{ij} + \beta(\nabla \cdot \mathbf{u})^2 \right] \tag{14}$$

3

It will be seen presently that these equations, though not in conservative form [9], are well suited to simulating highly compressible fluid motion.

4 Transport Coefficients

Along with the value given to the ratio of specific heats γ, a very important feature of any simulation of fluid dynamics is the set of values assigned to the dimensionless transport coefficients μ, μ_B, and κ. Although all of these coefficients vary with temperature and pressure, here they will be assumed to be constant. An investigation of the effects that their dependence on density and temperature may have will be deferred.

The values assigned to these dimensionless coefficients depend on both the physical references u_o, L_o, and T_o, and on numerical constraints, such as grid spacing. It is well known, for example, that the ratio of the largest dynamically important scales to the smallest is proportional to $Re^{3/4}$ [10]. Assuming that the constant of proportionality is about one, and since current computers limit the total number of points on a grid to about 10^6, we have $Re < 500$ for a three-dimensional grid and $Re < 10^4$ for a two-dimensional grid, approximately. Note that this is the Reynolds number based on a characteristic physical length, and not the microscale Reynolds number, which is based on an average turbulent eddy size. Other numerical constraints, such as a limit on available computational time, reduce grid sizes from their potential maximum and further reduce the maximum Re which may be considered.

However, once $\mu = 1/Re$ is set, the other transport coefficients follow somewhat directly. Since $Pr = \gamma\kappa/\mu \approx 1$ and since $1 < \gamma \leq 5/3$ for common gases, we see $\kappa \approx \mu$. The value of μ_B, or equivalently $\beta = \mu_B/\mu$, is highly dependent on whether the gas is polyatomic or not; although monatomic gases have $\beta \approx 0$, polyatomic gases range from $\beta \approx 1$ for air to $\beta \approx 30$ for molecular hydrogen to $\beta \approx 10^3$ for carbon dioxide [11].

5 Numerical Method

Here, we will use a Fourier pseudospectral technique [12] to numerically solve the logarithmic variable equations (12)–(14). In this method, the physical variables λ, $\mathbf{u}$, and σ are expanded in terms of discrete Fourier series, e.g.,

$$\lambda(\mathbf{x}) = \sum_{|\mathbf{k}|<N/2} \lambda(\mathbf{k})\, e^{i\mathbf{k}\cdot\mathbf{x}} \qquad (15)$$

The argument of the variable will be used to denote whether it is in x-space: $\lambda(\mathbf{x})$, or in k-space: $\lambda(\mathbf{k})$. In the above equation, n is the spatial dimension and N is the number of points on the numerical grid in one dimension (in 2D the grid is $N \times N$ and in 3D it is $N \times N \times N$). When discrete forward or inverse

Fourier transforms are needed, they are found using a fast Fourier transform (FFT) subroutine.

Notice that the maximum value of any component of $\mathbf{k}$ is strictly less than $N/2$. The reason is that a Fourier coefficient which has one of the components of $\mathbf{k}$ equal to $N/2$ has only a real part, as far as the FFT is concerned. Multiplying this component by $i\mathbf{k}$ yields the corresponding components of its gradient, for example, which have only imaginary parts. An FFT, however, ignores the imaginary part of such a component, so that its contribution to any derivative is always zero. It is therefore prudent to never include such components in any FFT-based method for the numerical solution of differential equations.

When the Fourier expansions of the physical variables are placed into the small set of partial differential equations (PDEs) (12)–(14), the result is a large set of ordinary differential equations (ODEs), one equation for every value of $\mathbf{k}$ which the FFT utilizes. Although either the set of PDEs in x-space or the set of ODEs in k-space can be time-integrated, here it is the ODEs which are integrated forward in time. The reason is that the numerical arrays in k-space contain fewer nonzero elements than the arrays in x-space. Since $|\mathbf{k}| < N/2$ and since the arrays in either space contain about N^n elements, then the ratio of nonzero array elements in k-space to x-space is $\pi/4 = 0.79$ in 2-D and $\pi/6 = 0.52$ in 3D (i.e., the ratio of the area of a circle to the area of the square which just encloses it, and the volume of a sphere to the volume of a cube which just encloses it, respectively). Thus, one may always reduce the size of a majority of the arrays in a k-space–based computer code so that they are *minimal* and yet contain all essential information. When it is necessary to perform an FFT to x-space, a minimal array is mapped into a full-sized FFT array; this is needed only to evaluate products of two x-space arrays, so only two full-sized FFT arrays are actually needed. Since the total number of arrays needed in a typical simulation are usually much greater than two, memory requirements in 2-D may be reduced by about 20% and in 3D by about 50%. (The argument in this paragraph also pertains to fully spectral methods where $|\mathbf{k}| < k_{max} < N/2$.)

Although minimal arrays are critical in order to maximize N, on modern supercomputers with very large memories such a large value of N may lead to prohibitively long run times. Since grid sizes are kept to a reasonable value in the work to be presented in this paper, minimal arrays are not used here (though they have been implemented previously [13]). Nonetheless, this is the motivation for solving the ODEs in k-space.

The time-integration method used here was a 'third-order partially corrected Adams-Bashforth scheme' [14]. The time-step size was variable and inversely proportional to the largest absolute modal value (R_{max}) from the right-hand-side of (12)–(14) at each iteration:

$$\Delta t = \begin{cases} \alpha/R_{max} & \text{if } R_{max} > 1 \\ \alpha & \text{if } R_{max} \leq 1 \end{cases} \tag{16}$$

where typically $10^{-2} \leq \alpha \leq 10^{-1}$. This method of determining Δt automatically

satisfies the necessary stability conditions [2].

In the pseudospectral method presented here, shock structure is resolved. This is done by considering cases where $\beta = \mu_B/\mu$ is large enough so that whatever shocks occur are of a naturally limited steepness [15]; for example, the gas under consideration can be H_2 (molecular hydrogen) or some mixture containing H_2, or the characteristic length L_o can be assumed small for an arbitrary polyatomic gas. In contrast, numerical solutions of the Euler equations require methods that use shock-capturing or shock-fitting [12, pp. 255–273].

6 Initial Conditions

In order to begin a simulation, the initial values of λ, $\mathbf{u}$, and σ need to be specified (but not the boundary conditions, which are periodic). The initial turbulent velocity is set according to

$$|\mathbf{u}(\mathbf{k})|^2 \sim k^4 \exp\left(-2k^2/k_o^2\right) \tag{17}$$

where k_o is the wave number at which the spectrum peaks; the phase of the $\mathbf{u}(\mathbf{k})$ are initially random. In setting the initial conditions on the velocity it is useful to decompose it into 'incompressible' and 'compressible' parts; in terms of Fourier coefficients, the decomposition is easily effected:

$$\mathbf{u}(\mathbf{k}) = \mathbf{u}^s(\mathbf{k}) + \mathbf{u}^c(\mathbf{k}) \tag{18}$$

where the solenoidal (i.e, incompressible) part $\mathbf{u}^s$ and compressible part $\mathbf{u}^c$ are,

$$\mathbf{u}^s(\mathbf{k}) = (\mathbf{I} - \hat{\mathbf{k}}\hat{\mathbf{k}}) \cdot \mathbf{u}(\mathbf{k})$$
$$\mathbf{u}^c(\mathbf{k}) = \hat{\mathbf{k}}\hat{\mathbf{k}} \cdot \mathbf{u}(\mathbf{k}) \tag{19}$$

and where $\hat{\mathbf{k}}$ is the unit vector in the direction of $\mathbf{k}$. The $\mathbf{k} = 0$ component of $\mathbf{u}^s$ corresponds to the mean flow velocity.

For the moment assume that we have an initially incompressible flow. Then $\mathbf{u}^c = 0$ and $\rho = 1$ at $t = 0$; upon taking the divergence of (10) and defining $T = 1 + T'$, we find the fluctuation T' initially satisfies:

$$-\nabla^2 T' = \gamma \, \partial_i \partial_j u_i^s u_j^s$$
$$= S(\mathbf{x}) \tag{20}$$

In terms of Fourier coefficients, the temperature fluctuations which are consistent with the assumption of an initially incompressible flow are given by

$$T'(\mathbf{k}) = k^{-2} S(\mathbf{k}) \quad \text{where } k > 0 \tag{21}$$

Since $T'(\mathbf{x}) > -1$ in order that $T > 0$, and since $T' \sim \gamma|\mathbf{u}^s|^2$, then $\mathbf{u}^s$ must be scaled accordingly. The mean value of $|\mathbf{u}^s|^2$ (denoted by $\langle|\mathbf{u}^s|^2\rangle$) is the initial turbulent Mach number squared M_t^2. The maximum fluctuation of $|\mathbf{u}^s|^2$

6

is larger than M_t^2, and we expect that $\max M_t \sim \gamma^{-1}$ in order that the constraint $T' > -1$ is obeyed. Here, when initial flow conditions with close to maximal incompressible velocities are desired, the initial velocity is scaled so that $\min T'(\mathbf{x}) = -0.99$.

In truly incompressible initial conditions, the flow is subsonic. However, we are at liberty to choose λ, $\mathbf{u}$, and σ *arbitrarily* as initial conditions for the Navier-Stokes equations. Thus, supersonic ($\max|\mathbf{u}(\mathbf{x})| > 1$) initial turbulent flow conditions can be specified. For example, $\lambda(\mathbf{k})$, $\mathbf{u}^c(\mathbf{k})$, $\mathbf{u}^s(\mathbf{k})$, and $\sigma(\mathbf{k})$ can be specified *independently* of one another. As another example, an initially incompressible flow field can be specified (to represent a local region of turbulence) and a compressible flow field (corresponding to an approaching shock front) can be added to it. These alternatives will, in fact, enable us to investigate highly compressible homogeneous turbulence and shock-turbulence interactions.

7 Numerical Results

The pseudospectral logarithmic variable method was implemented in both a 3D code and a 2D code. The 3D code was used to simulate supersonic isotropic turbulence on a 64^3 grid, while the 2D code was used to examine the passage of a region of turbulent flow through a shock on a 512^2 grid. These numerical studies will be discussed following the definition of some quantitative flow measures.

It will be useful at this point to define a number of quantities which measure certain characteristics of a turbulent flow and its simulation. First, the mean of a quantity Q averaged over its values at all grid points $\mathbf{x}_i$ will be denoted by

$$\langle Q \rangle \;=\; \frac{1}{N^n} \sum_i Q(\mathbf{x}_i) \tag{22}$$

where $n = 2$ for 2D and $n = 3$ for 3D. The turbulent Mach number M_t, average wavenumber k_{ave}, dissipation wavenumber k_D, microscale Reynolds number R_λ and compressibility index χ are then

$$
\begin{aligned}
M_t &= \left(\langle |\mathbf{u}|^2 \rangle / \langle T \rangle \right)^{1/2} \\
k_{ave} &= \left[\langle (\partial_i u_j)^2 \rangle / \langle u_i u_i \rangle \right]^{1/2} \\
k_D &= \left(\langle \varepsilon \rangle / \langle \mu^3 \rangle \right)^{1/4} \\
R_\lambda &= \langle |\mathbf{u}|^2 \rangle^{1/2} \lambda_{ave} / \nu \\
\chi &= \langle |\mathbf{u}^c|^2 \rangle / \langle |\mathbf{u}|^2 \rangle
\end{aligned}
\tag{23}
$$

In the dimensionless system adopted here, $\nu = \mu$. Also, $\lambda_{ave} = 2\pi/k_{ave}$ and the local dissipation rate ε is

$$\varepsilon \;=\; \mu \left[(\nabla \times \mathbf{u})^2 + (\beta + 4/3)(\nabla \cdot \mathbf{u})^2 \right] \tag{24}$$

Dissipation clearly has a part related to vorticity $\nabla \times \mathbf{u}$ and to dilatation $\nabla \cdot \mathbf{u}$.

7.1 3D Homogeneous Supersonic Turbulence

In the previously cited work [2–7], initial RMS Mach numbers were never above $M_t = 0.8$, and usually were much less. One possible reason for this limitation is the occurrence of negative values of density or temperature on the numerical grid, which can lead to such local instabilities as effectively negative diffusion. Here, these possibilities are explicitly avoided through the use of logarithmic variables. The initial RMS Mach number for the test cases considered ranged from $M_t = 1$ to $M_t = 2$ and there were no problems experienced in these 64^3 simulations (such as conservation of energy) as long as the dissipation wave number began and remained less than $k_{max} = 32$.

Consider two cases for which $M_t = 1$ initially; in these cases, half of the physical volume contains flow with supersonic velocity at $t = 0$. In both cases, $\gamma = 1.4, \mu = 0.01, \beta = 0$, and $\kappa = 0.7$ (the Prandtl number is thus approximately unity); these values correspond roughly to those of air. Also at $t = 0$, $\lambda = \sigma = 0$ everywhere and the velocity satisfied (17), with $k_o = 6$.

The difference between the two runs lay in the value of χ. In run 3D64A, $\chi = 0.25$ while in run 3D64B, $\chi = 0.75$ at $t = 0$. Both simulations ran until almost $t = 1$ at about 14 cpu-sec/Δt; the fluctuation in total energy was less than 0.2% for 3D64A and less than 0.5% for 3D64B. In Figures 1 and 2, the time variation of the quantities M_t and χ, and in Figures 3 and 4, the time variations of R_λ, k_{ave}, and k_D are shown for runs 3D64A and 3D64B, respectively. For these runs, $k_D < k_{max} = 32$, so that both are numerically well resolved.

One difference between the two runs manifests itself in the evolution of enstrophy $\langle (\nabla \times \mathbf{u})^2 \rangle$ and mean square divergence $\langle (\nabla \cdot \mathbf{u})^2 \rangle$. These quantities are are presented in Figures 5 and 6 for runs 3D64A and 3D64B, respectively. Since $\beta = 0$ for these runs, a consideration of (24), along with Figures 5 and 6, shows that dissipation occurs primarily due to vortical motion, rather than to dilatational motion (although for a short time after the start of run 3D64B dilatational motion is actually more important).

Another difference is in the relation between the solenoidal and compressible velocity spectra, as shown in Figures 7 and 8, for runs 3D64A and 3D64B, respectively. Figures 7 and 8, which correspond to $t = 0.57$ and $t = 0.56$, respectively, show that the dominant part of the velocity spectra at the highest k-values is the compressible one. However, Figure 8, corresponding to run 3D64B which had an initial value of $\beta = 0.75$, indicates that the compressible part of the velocity spectra is also dominant over the medium as well as high k-values.

7.2 2D Shock-Turbulence Interaction

In addition to the homogeneous 3D runs just described, a set of 2D runs on a 512^2 grid were completed. These runs, 2D512A, 2D512B, and 2D512C, differed initially only in the value of β assigned to each: 10, 30, and 100, respectively; for all three runs, $\mu = 0.001, \kappa = 0.7$, and $\gamma = 1.4$. All the runs began

with identical initial conditions, which consisted of a region of incompressible turbulence satisfying (17) with $k_o = 9$ filling the left half of the 2D grid and a shock wave in the right half of the grid. Using the shock jump conditions [10, p. 335], density, temperature, and velocity corresponding to a Mach 2 shock were set inside the right half of the grid, while in the left half of the grid the mean density was $< \rho >= 1$ and the mean velocity was $< u_x >= 2$ (the frame of reference was such that the shock front was initially stationary and the turbulent region was moving from left to right into it). At the edges of the turbulent region, there were transition regions of twenty grid points in the x-direction (i.e., the streamwise direction) in which the interior turbulent velocity field went smoothly to zero (by a squared-cosine taper). The turbulent temperature fluctuations were determined by (21).

Similarly, there was a squared-cosine taper from the free stream values of density, temperature, and velocity to their jump values, and back again, over the twenty grid points on the outside edges of the shocked region. Thus, we begin on the leftmost edge of the grid with freestream values, make a transition into a turbulent region, make another transition out of the turbulent region back into the freestream values and then a transition into the shocked region, followed by a transition back to freestream values on the rightmost edge of the grid. This resulted in a periodic set of initial conditions which could be treated by a Fourier method. These initial conditions can be thought of as 1) a one-dimensional Mach 2 shock wave, and 2) a localized region of eddy turbulence placed into the freestream flow (and moving with it) just ahead of the shock front.

Once evolution began, the front of the shock steepened slightly, and the density and temperature increased slightly, leading to a pressure jump ratio of 5 across the shock front (it was initially 4.5). Based on this pressure ratio the Mach number of the shock should have risen to 2.1; the shock front, which would have remained stationary in the reference frame chosen, was observed to move forward at a relative velocity of 0.1, in accordance with expectations. During the same time, the back of the initial shock pulse spread into a rarefaction wave. As an example of the time variation of R_λ, k_D, and k_{ave}, consider Figure 9, which pertains to run 2D512B, and is similar for the other 2D runs. Since $k_D < k_{max} = 256$, it would appear that the turbulence is sufficiently well resolved.

The resolution of the shock front, in turn, gets better with increasing values of β. Consider Figures 10, 11, and 12, where spanwise averages for vorticity and pressure are shown for the three runs for the same time ($t = 0.567$). In Figure 10, which corresponds to $\beta = 10$, there are some oscillations in the shock front; these oscilations disappear, however, in the Figures 11 and 12, which correspond to $\beta = 30$ and $\beta = 100$, respectively. To visualize what happens to the turbulence as it crosses the shock front, consider Fiqures 13 and 14, which show a small section of the grid for runs 2D512A and 2D512B ($\beta = 10$ and $\beta = 30$, respectively), both at $t = 0.567$.

9

In Figures 11 and 12, the vorticity jumps by a factor of about 2.5, which is also the case for Figure 10, if the initial overshoot is ignored. This is consistent with linear theory [16, 17]. The shape of the shocks is also consistent with the results from previous simulations using *ENO* methods [18].

8 Conclusion

In this paper, two primary extensions of pseudospectral Fourier methods for solving the compressible Navier-Stokes equations have been described. First, by using a 'logarithmic variable' formulation of the basic equations, it was shown that supersonic homogeneous turbulence could easily be simulated. Second, by using realistic values of the ratio of bulk viscosity to shear viscosity, it was demonstrated that shock structure could be resolved and shock-turbulence interactions could be examined by direct numerical simulation.

The logarithmic variable method is not an explicitly conservative formulation, though it was seen that the global energy was very well conserved. In addition, the Rankine-Hugoniot relation between pressure jump across a shock and upstream Mach number was also seen to hold. Although these measures indicate that the numerical method was accurately solving the equations of motion, an exhaustive study was not performed. Such a study is more appropriately done in a one-dimension simulation, rather than the two- and three-dimensional simulations presented here, and will be deferred.

Note that shock capture and resolution is facilitated by the naturally occurring bulk viscosity term. It had been found in pioneering work in the numerical solution of flow problems involving shocks [9], that the introduction of an 'artificial viscosity' was necessary to ensure numerical stability in solving the Euler equations. Other viable stabilization techniques for the Euler equations, including spectral filtering and smoothing, have also been developed [19]. In addition to these techniques for Euler flows, 'hyperviscosity' methods have been applied in solving compressible Navier-Stokes flows, for the purpose of increasing the effective Reynolds number of a simulation, as well as ensuring stability [20]. In comparison to these *algorithmic* approaches, the novelty here is, again, that we use a *physically* motivated approach involving the bulk viscosity. It may prove useful to compare these different methods in greater detail, but this is beyond the scope of the present work.

Although the distribution of grid points is not concentrated at the shock front, this is not a disadvantage. In particular, the presence of turbulence also requires a sufficient number of grid points for its resolution; thus it is advantageous to have an even distribution of grid points, since small scale dynamic activity is occuring at essentially all parts of the grid. In this way, the small scale structure of turbulence and the small scale structure of shock fronts are treated equally.

In the future, we hope to incorporate reacting flows within the kind of sim-

ulations described here. This is an important application, since a turbulent, reacting flow, in the presence of shocks, occurs in many situations of interest to the aerospace and astrophysical communities. One specific area of interest is in the supersonic, turbulent combustion which occurs in a scramjet engine. Another is the inflow through the accretion shock around a black hole.

9   Acknowledgements

References

[1] J. E. Moyal, 'The spectra of turbulence in a compressible fluid; eddy turbulence and random noise,' *Math. Proc. Cambridge Philos. Soc.*, **48**, 329–344, 1952.

[2] T. Passot and A. Pouquet, 'Numerical simulation of compressible homogeneous flows in the turbulent regime,' *J. Fluid Mech.*, **181**, 441–446, 1987.

[3] G. Erlebacher, M. Y. Hussaini, H. O. Kreiss, and S. Sarkar, 'The analysis and simulation of compressible turbulence,' *Theor. Comput. Fluid Dyn.*, **2**, 73–95, 1990.

[4] G. A. Blaisdell, N. N. Mansour, and W. C. Reynolds, 'Numerical simulations of compressible homogeneous turbulence,' *Report No. TF-50*, Stanford Univ., 1991.

[5] S. Sarkar, G. Erlebacher, and M. Y. Hussaini, 'Direct simulation of compressible turbulence in a shear flow,' *Theor. Comput. Fluid Dyn.*, **2**, 291–305, 1991.

[6] S. Kida and S. Orszag, 'Energy and spectral dynamics in decaying compressible turbulence,' *J. Sci. Comp.*, **7**, 1–34, 1992.

[7] T. A. Zang, R. B. Dahlburg, and J. P. Dahlburg, 'Direct and large eddy simulations of three-dimensional compressible turbulence,' *Phys. Fluids A*, **4**, 127–140, 1992.

[8] J. V. Shebalin and D. Montgomery, 'Turbulent magnetohydrodynamic density fluctuations,' *J. Plasma Phys.*, **39**, 339-367, 1988.

[9] R. D. Richtmeyer and K. W. Morton, *Difference Methods for Initial Value Problems*, 2nd Ed., pp. 300–338, Interscience, New York, 1967.

11

[10] L. D. Landau and E. M. Lifshitz, *Fluid Mechanics*, 2nd Ed., p. 134, Pergamon, Oxford, 1987.

[11] P. A. Thompson, *Compressible-Fluid Dynamics*, p. 30, McGraw-Hill, New York, 1972.

[12] C. Canuto, M. Y. Hussaini, A. Quateroni, and T. A. Zang, *Spectral Methods in Fluid Dynamics*, p. 83, Springer-Verlag, New York, 1988.

[13] J. V. Shebalin, 'Magnetic field amplification in mechanically driven magnetohydrodynamic turbulence,' *AIAA Journal*, **28**, 1360-8, 1990.

[14] J. Gazdag, 'Time-differencing schemes and transform methods,' *J. Comp. Phys.*, **20**, 196-207, 1976.

[15] D. Gilbarg and D. Paolucci, 'The structure of shock waves in the continuum theory of fluids,' *J. Rat. Mech. Anal.*, *2*, 617-642, 1953.

[16] H. S. Ribner, 'Spectra of noise and amplified turbulence emanating from shock-turbulence interaction,' *AIAA Journal*, **25**, 436-442, 1987.

[17] S. Lee, S. K. Lele, and P. Moin, 'Direct numerical simulation of shock turbulence interaction,' *AIAA 91-0523*, 29th Aerospace Sciences Mtg., Reno, NV, 1991.

[18] R. Hannappel and R. Friedrich, 'Interaction of isotropic turbulence with a normal shock wave,' 2nd Euroturbulence Conf., Delft, Holland, 1992.

[19] M. Y. Hussaini, D. A. Kopriva, M. D. Salas, and T. A. Zang, 'Spectral methods for the Euler equations: Part 1-Fourier methods and shock capturing,' *AIAA Journal*, **23**, 64-70, 1985.

[20] T. Passot and A. Pouquet, 'Hyperviscosity for compressible flows using spectral methods,' *J. Comp. Phys.*, **75**, 300-313, 1988.
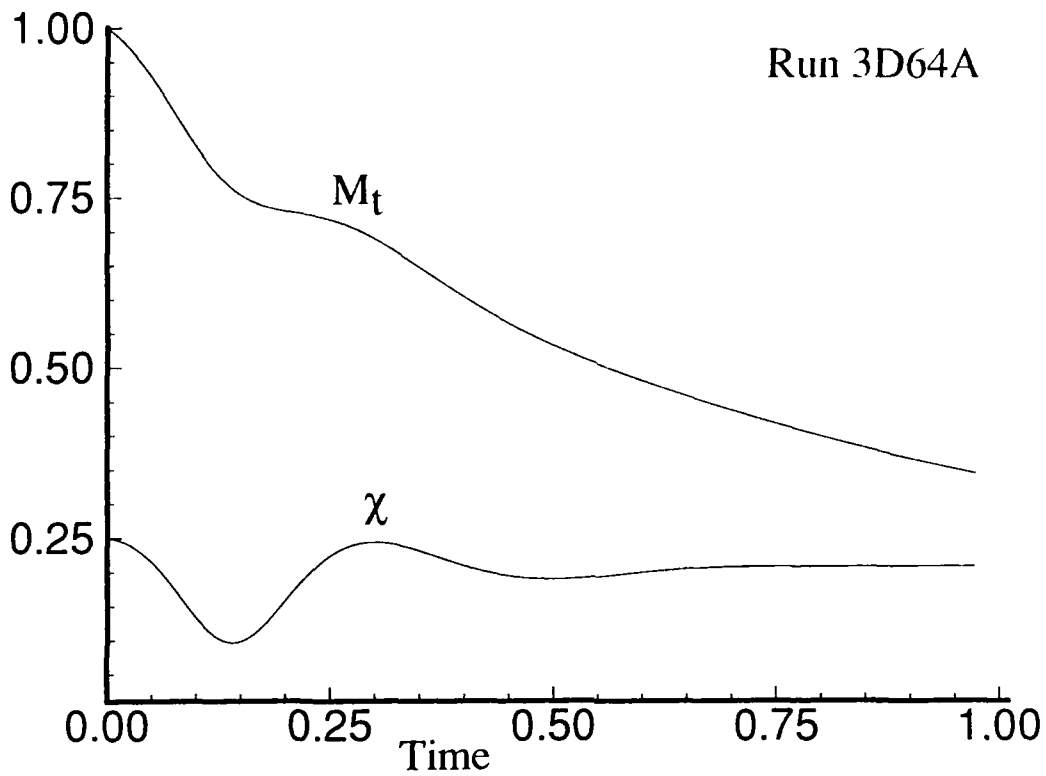
Figure 1. RMS Mach number M_t and compressibility index χ for run 3D64A.
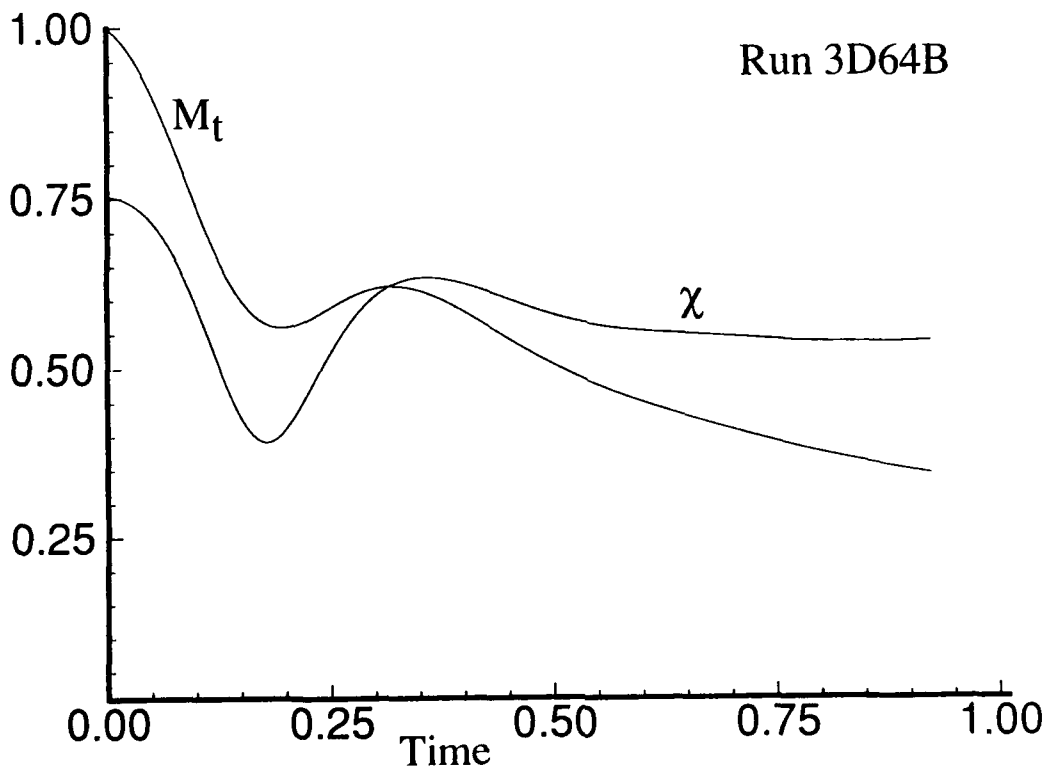
Figure 2. RMS Mach number M_t and compressibility index χ for run 3D64B.
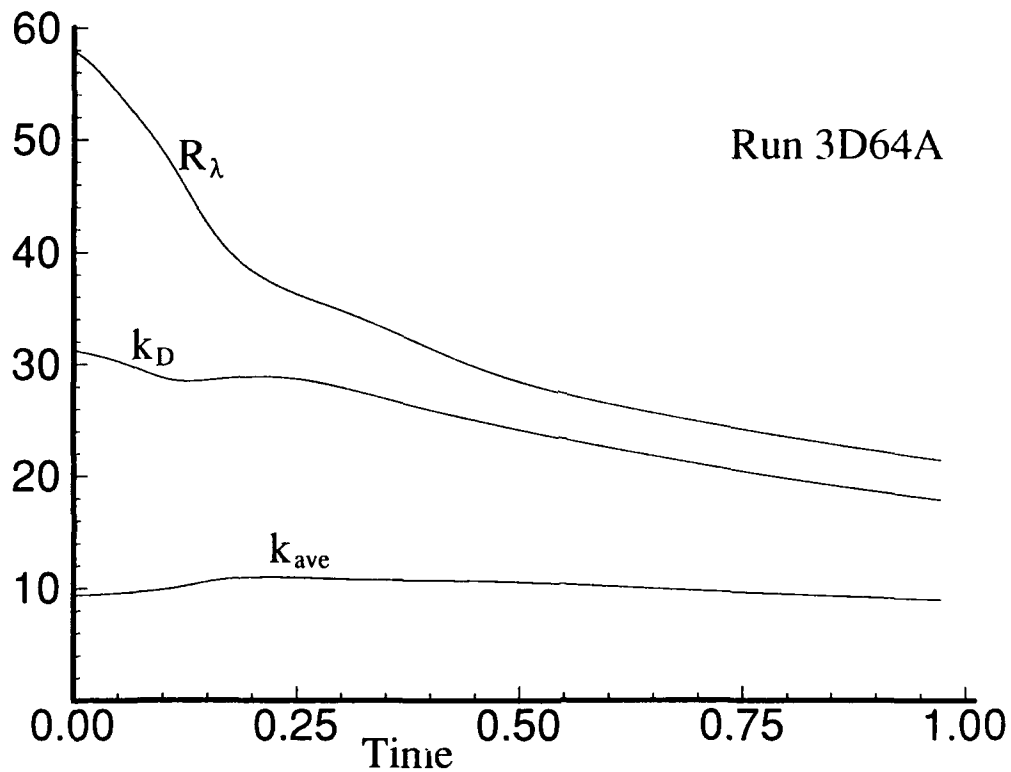
13

Figure 3. Microscale Reynolds number R_λ, average wave number k_{ave}, and dissipation wave number k_D for run 3D64A.
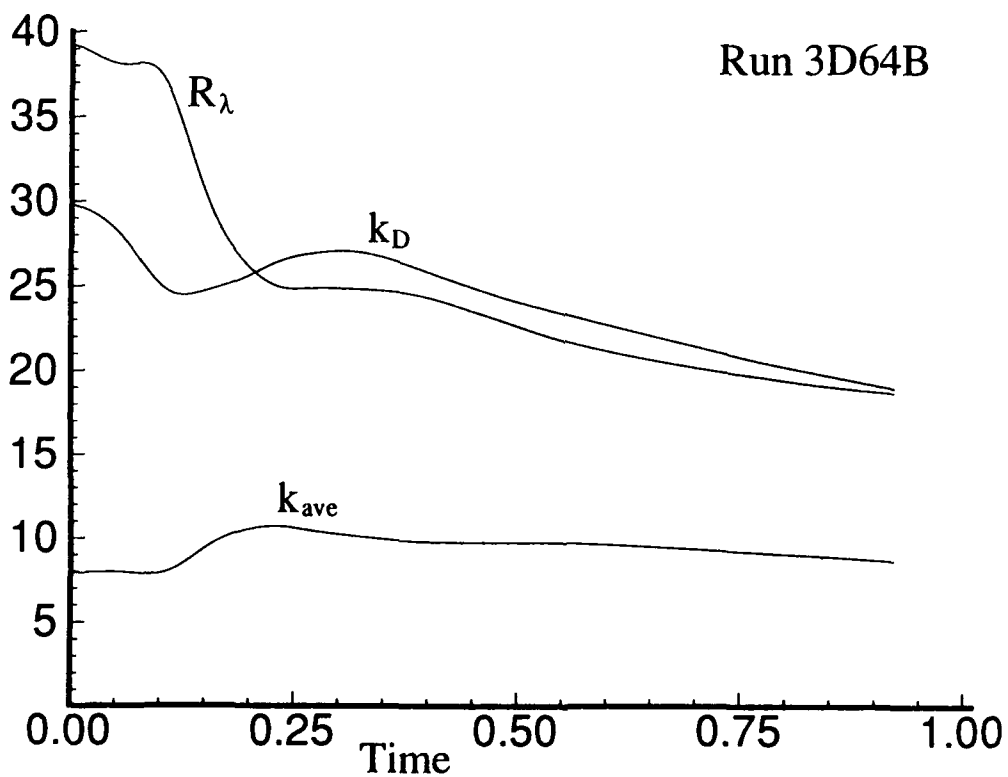

Figure 4. Microscale Reynolds number R_λ, average wave number k_{ave}, and dissipation wave number k_D for run 3D64B.
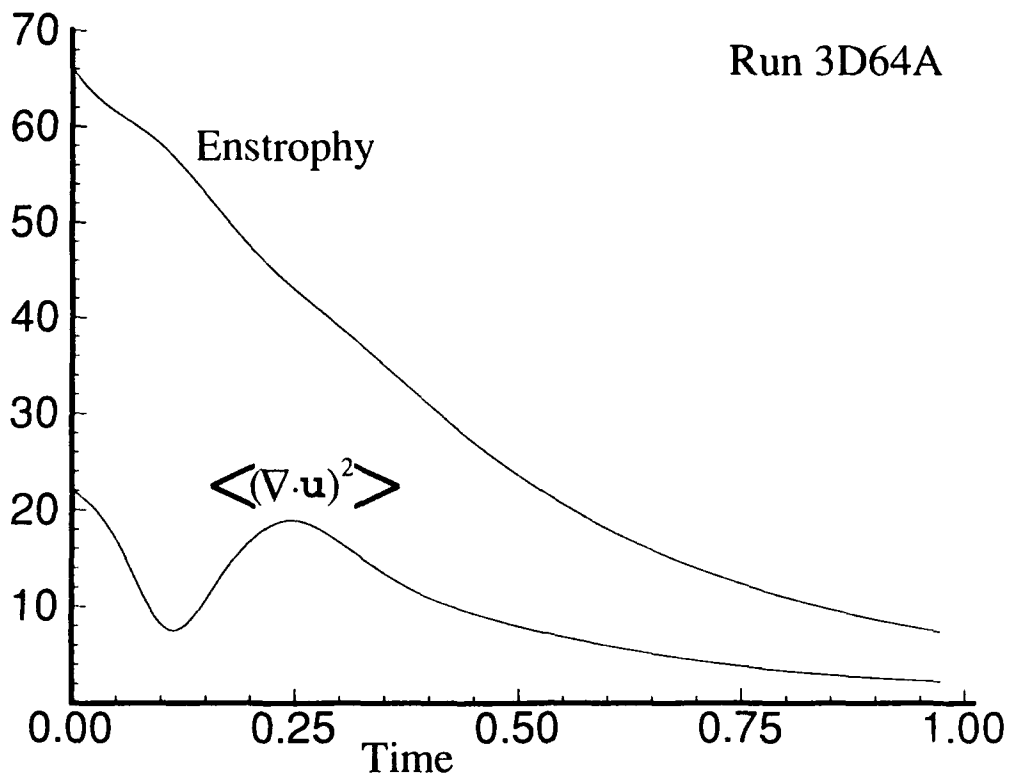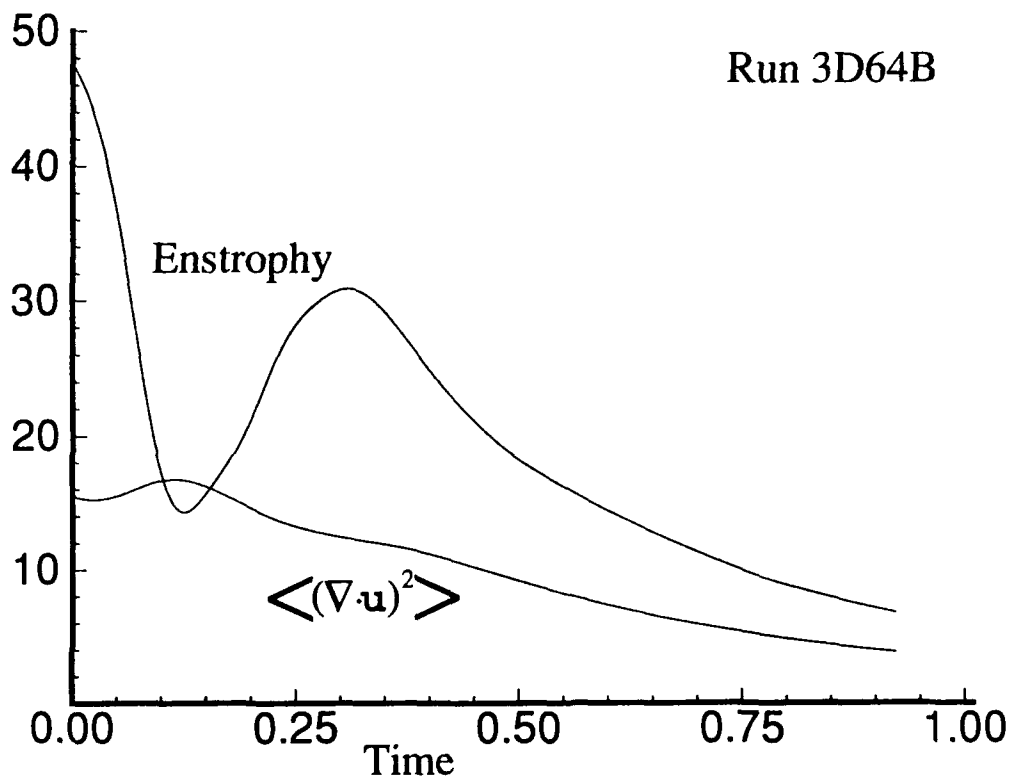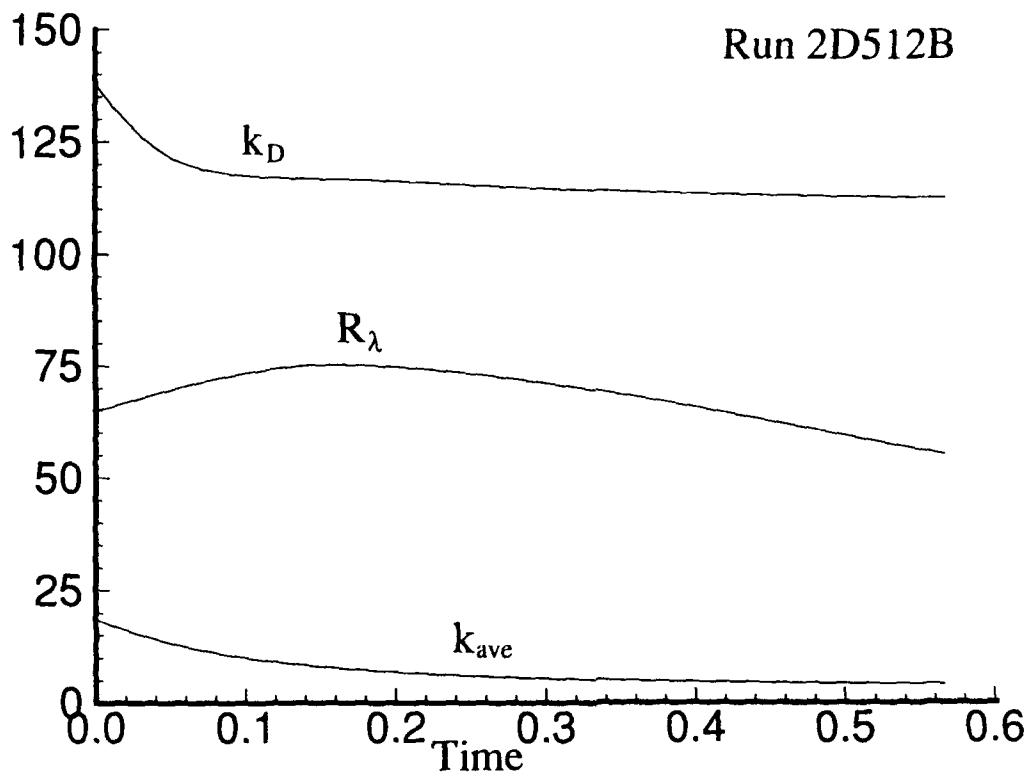
Figure 5. Enstrophy and mean square divergence for run 3D64A.

Figure 6. Enstrophy and mean square divergence for run 3D64B.
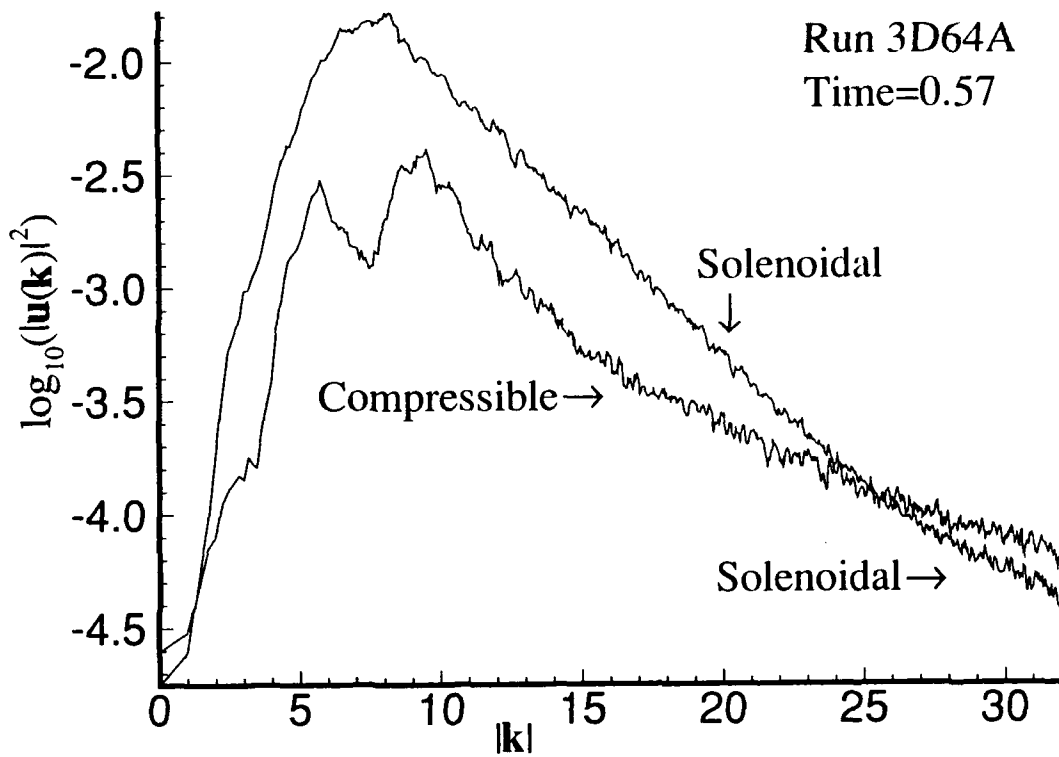
Figure 7. Solenoidal and compressible velocity spectra for run 3D64A.
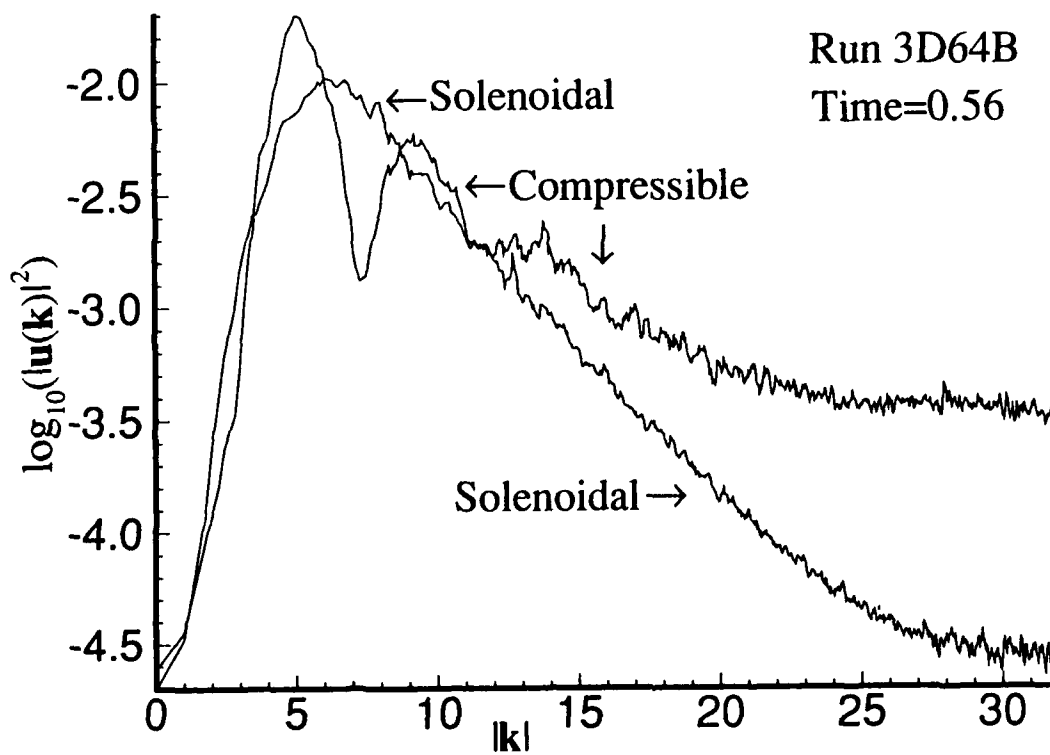
Figure 8. Solenoidal and compressible velocity spectra for run 3D64B.

Figure 9. Microscale Reynolds number R_λ, average wave number k_{ave}, and dissipation wave number k_D for run 2D512B.
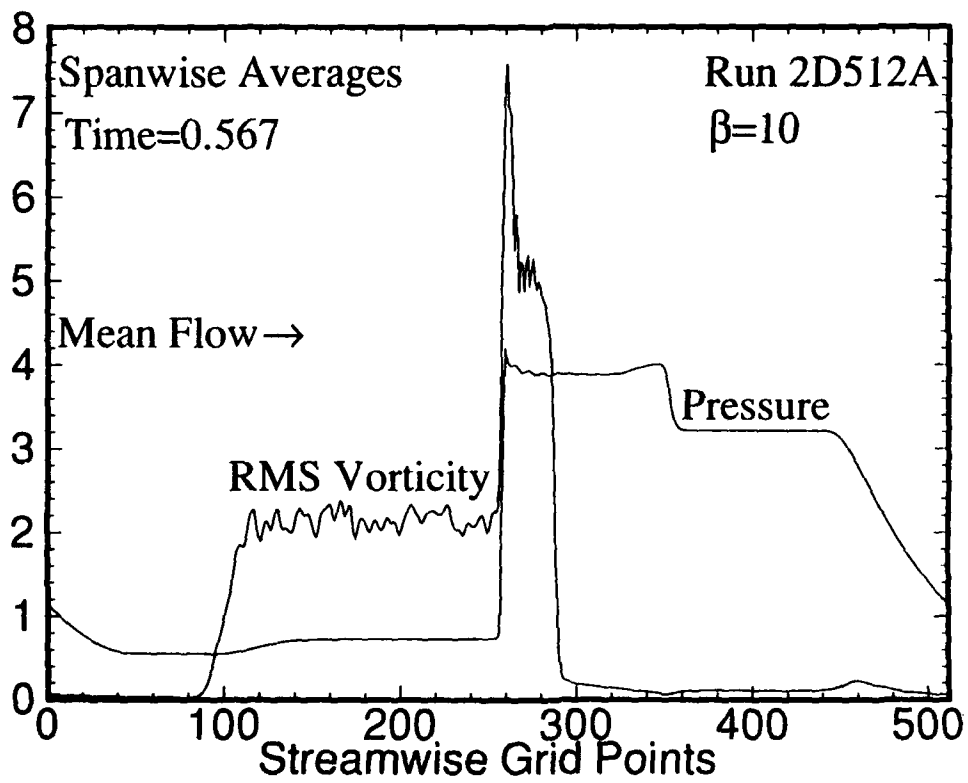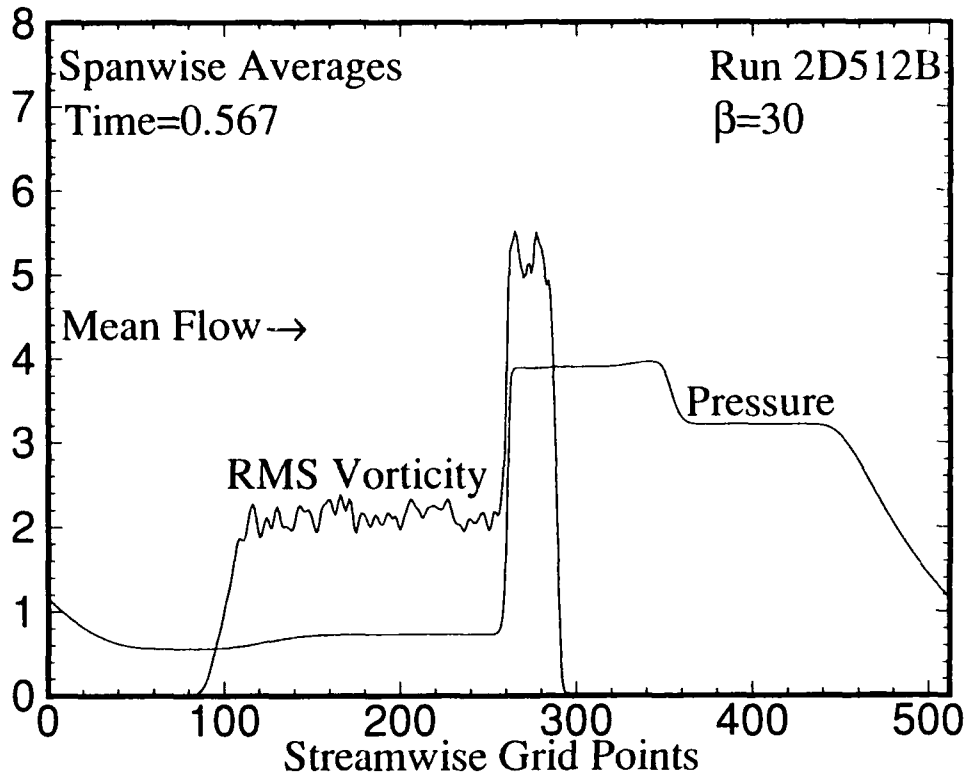

Figure 10. Spanwise averages for pressure and RMS vorticity for run 2D512A.

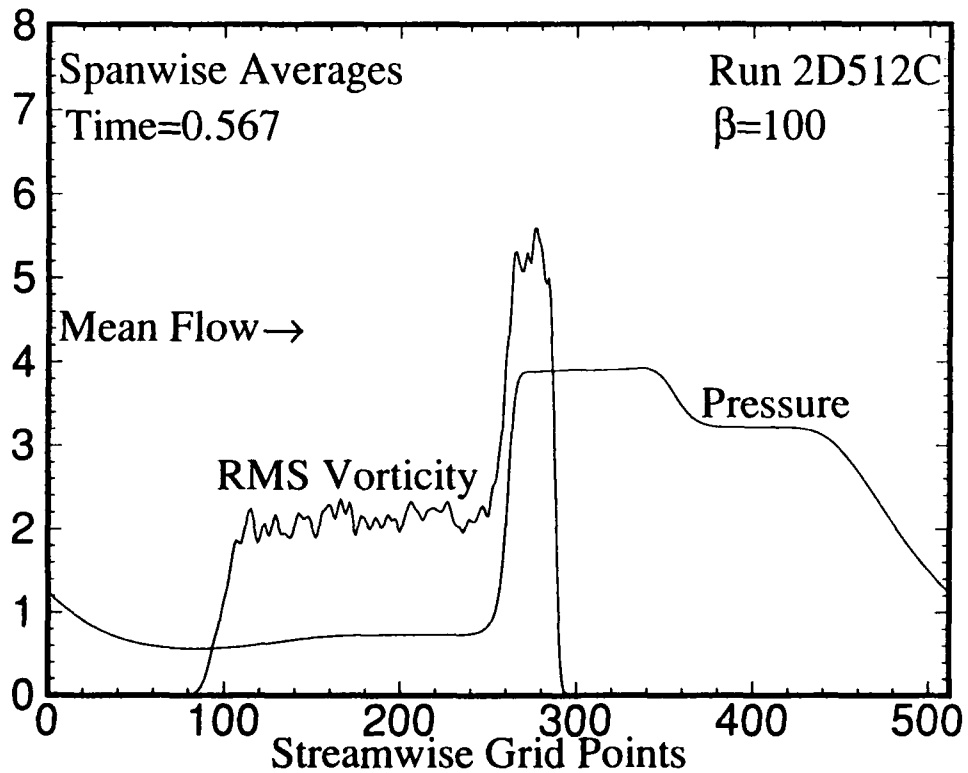Figure 11. Spanwise averages for pressure and RMS vorticity for run 2D512B.

Figure 12. Spanwise averages for pressure and RMS vorticity for run 2D512C.

18

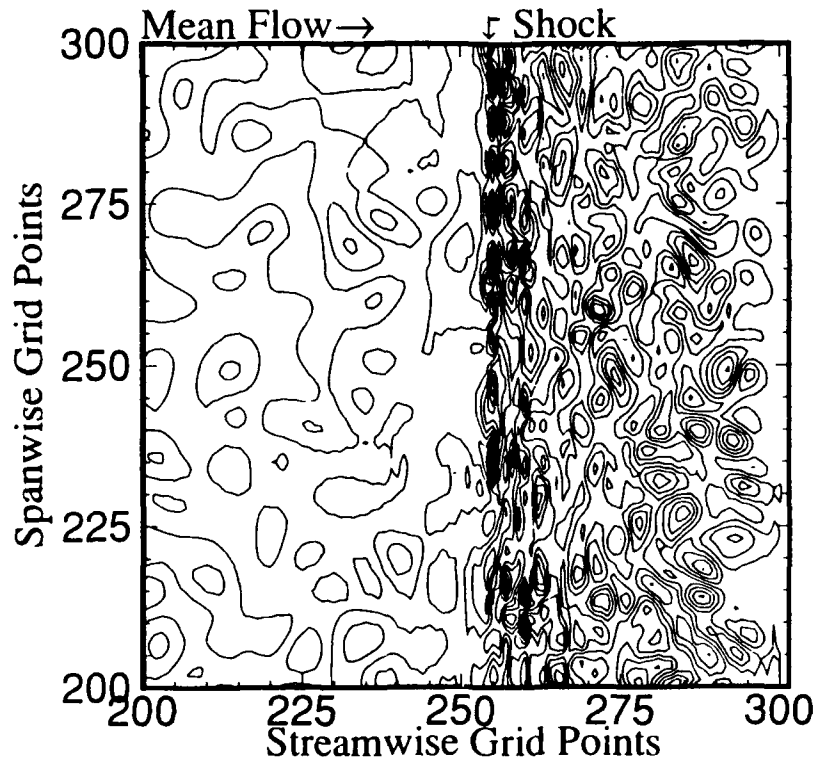## Vorticity Contours for Run 2D512A at t=0.749

Figure 13. Vorticity contours for a small section of run 2D512A.
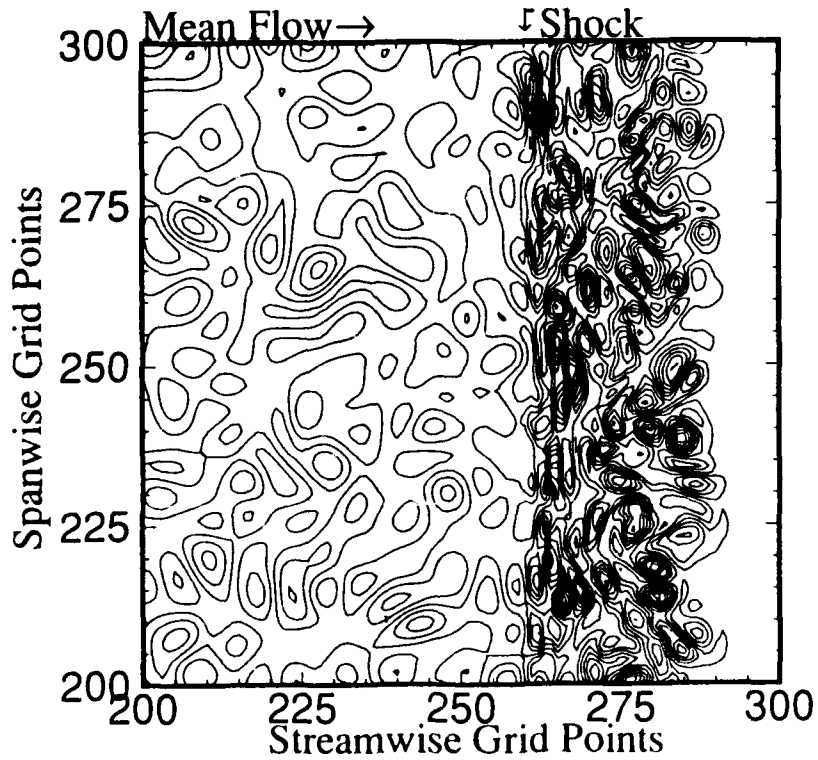
Vorticity Contours for Run 2D512B at t=0.567

Figure 14. Vorticity contours for a small section of run 2D512B.

REPORT DOCUMENTATION PAGE

Public reporting burden for this collection of information is estimated to average 1 hour per response, including the time for reviewing instructions, searching existing data sources, gathering and maintaining the data needed, and completing and reviewing the collection of information. Send comments regarding this burden estimate or any other aspect of this collection of information, including suggestions for reducing this burden, to Washington Headquarters Services, Directorate for Information Operations and Reports, 1215 Jefferson Davis Highway, Suite 1204, Arlington, VA 22202-4302, and to the Office of Management and Budget, Paperwork Reduction Project (0704-0188), Washington, DC 20503.

1. AGENCY USE ONLY (Leave blank)	2. REPORT DATE January 1993	3. REPORT TYPE AND DATES COVERED Technical Memorandum

4. TITLE AND SUBTITLE PSEUDOSPECTRAL SIMULATION OF COMPRESSIBLE TURBULENCE USING LOGARITHMIC VARIABLES	5. FUNDING NUMBERS WU 505-90-52-01
6. AUTHOR(S) John V. Shebalin	

7. PERFORMING ORGANIZATION NAME(S) AND ADDRESS(ES) NASA Langley Research Center Hampton, VA 23681-0001 and Institute for Computer Applications in Science 　and Engineering NASA Langley Research Center, Hampton, VA 23681-0001	8. PERFORMING ORGANIZATION REPORT NUMBER ICASE Report No. 92-61

9. SPONSORING/MONITORING AGENCY NAME(S) AND ADDRESS(ES) National Aeronautics and Space Administration Washington, DC 20546-0001	10. SPONSORING/MONITORING AGENCY REPORT NUMBER NASA TM-107707 ICASE Report No. 92-61

12a. DISTRIBUTION/AVAILABILITY STATEMENT Unclassified - Unlimited Subject Category 34	12b. DISTRIBUTION CODE

13. ABSTRACT (Maximum 200 words)

The direct numerical simulation of dissipative highly compressible turbulent flow is performed using a pseudospectral Fourier technique. The governing equations are cast in a form where the important physical variables are the fluid velocity and the natural logarithms of the fluid density and temperature. Bulk viscosity is utilized to model polyatomic gases more accurately and to ensure numerical stability in the presence of strong shocks. Numerical examples include three-dimensional supersonic homogeneous turbulence and two-dimensional shock-turbulence interactions.

14. SUBJECT TERMS direct numerical simulation; sompressible turbulence			15. NUMBER OF PAGES 21
			16. PRICE CODE A03

17. SECURITY CLASSIFICATION OF REPORT Unclassified	18. SECURITY CLASSIFICATION OF THIS PAGE Unclassified	19. SECURITY CLASSIFICATION OF ABSTRACT	20. LIMITATION OF ABSTRACT

National Aeronautics and
Space Administration
Code JTT
Washington, D.C.
20546-0001
Official Business
Penalty for Private Use, $300

NASA

POSTMASTER: If Undeliverable (Section 158
Postal Manual) Do Not Return